

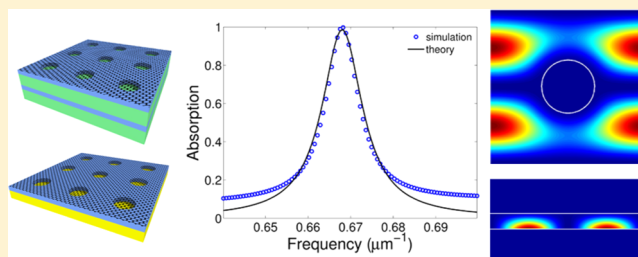
Total Absorption in a Graphene Monolayer in the Optical Regime by Critical Coupling with a Photonic Crystal Guided Resonance

Jessica R. Piper* and Shanhui Fan*

Ginzton Laboratory, Department of Electrical Engineering, Stanford University, Stanford, California 94305, United States

ABSTRACT: We numerically demonstrate total absorption in graphene in the near-infrared and visible wavelength ranges by means of critical coupling with guided resonances of a photonic crystal slab. In this wavelength range, there is no plasmonic response in undoped graphene, so the critical coupling is entirely controlled by the properties of the photonic crystal resonance. We discuss the general theory and conditions for absorption enhancement and critical coupling in a thin film and give design rules for a totally absorbing system. We present examples in the near-infrared and visible, using both a lossless metallic mirror and a realistic multilayer dielectric mirror.

KEYWORDS: graphene, photonic crystal, near-infrared, critical coupling, guided resonance, absorption enhancement



Over the past decade, graphene has been intensively studied due to its unique electronic and optical properties.^{1–3} Graphene exhibits remarkably high absorption for an atomically thin layer (~ 0.34 nm thickness), but in order to realize many high-performance graphene-based optical devices,^{4–6} enhancement of absorption up to 100% is highly desirable.

Absorption enhancement of graphene has been studied extensively in both the visible/near-infrared and the mid- to far-infrared. In the mid- to far-infrared (corresponding to a free-space wavelength range of approximately 5 – 100 μm), graphene exhibits a strong plasmonic response.² The plasmon modes can be accessed from free space by use of a grating coupler, where an unpatterned graphene monolayer is deposited on a subwavelength dielectric grating.^{7–9} Alternately, by shaping the graphene into ribbons¹⁰ or disks,¹¹ localized surface plasmon modes can be excited. In the latter case, absorption at resonance reaching 100% has been demonstrated numerically. By combining patterned graphene and the high doping achievable with the use of ionic liquids, plasmonic response at wavelengths approaching 3 μm has been observed.¹²

In contrast, in the visible and near-infrared ($\lambda < 2$ μm), the plasmonic response is absent for undoped, unpatterned graphene.¹³ In this wavelength range, the absorption of monolayer graphene is defined by the fine structure constant $\alpha = e^2/\hbar c$, giving a single-pass absorption $A = \pi\alpha \approx 2.3\%$.¹⁴ In order to significantly enhance absorption in this wavelength regime, one can place graphene near plasmonic nanoantennas¹⁵ or place the graphene inside a resonant Fabry–Perot cavity.^{16,17} While graphene inside a cavity can exhibit perfect absorption, fabrication is challenging due to the need to build a multilayer dielectric mirror on top of the graphene.

In this work, we investigate total absorption in graphene by critical coupling¹⁸ to a guided resonance^{19–25} of a photonic crystal slab, in the visible and near-infrared regime, where

graphene does not have any plasmonic response. The geometry, shown schematically in Figure 1, consists of

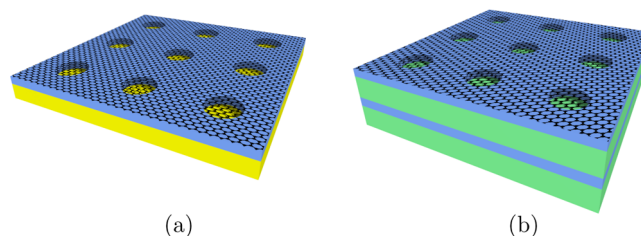


Figure 1. Schematic of an absorption enhancement system for graphene, using either (a) a lossless metallic mirror or (b) a multilayer dielectric Bragg mirror (1.5 pairs are shown). The high-index dielectric is blue, yellow represents the lossless metal, and green represents a low-index dielectric. In both cases, light is incident normally from above. The photonic crystal is described by its thickness d , lattice period Λ , and hole radius r .

monolayer graphene on top of a photonic crystal slab, backed by a mirror. The photonic crystal is composed of a square lattice of air holes in a high-index dielectric. When the leakage rate of a mode out of the slab is equal to the absorption rate of that mode in the graphene, the system is said to be *critically coupled*, and all the incident light is absorbed. We note that a similar structure has been studied in the mid- and far-infrared regimes. References 7–9, however, exploit the dielectric grating to couple into the plasmon modes of graphene in the mid- and far-infrared. In contrast, for our range of wavelengths studied, the lack of graphene plasmons results in a design and underlying physics that are significantly different.

Received: October 29, 2013

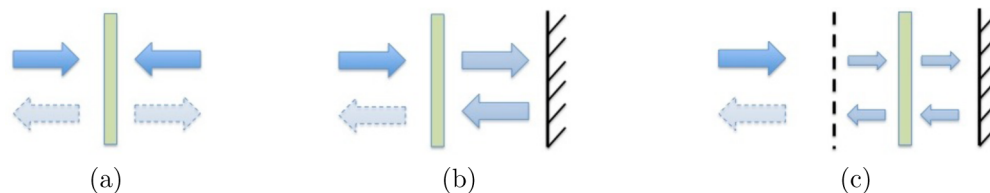


Figure 2. One-dimensional geometries for total absorption in a thin film, in order of increasing complexity. In each case, coherent interference causes cancellation of the shaded outgoing wave(s). (a) Geometry for a coherent perfect absorber, where both input beams are totally absorbed. (b) Critical coupling of a thin film with dielectric spacer and perfect mirror. (c) The film inside a Fabry–Perot cavity with partially transmitting front mirror ($|r| < 1$) and perfect back mirror.

Using the structures shown in Figure 1, with the photonic crystal made of silicon, we show that total absorption can be achieved in monolayer graphene at $1.5 \mu\text{m}$. Total absorption is achievable using either a lossless metallic mirror or a realistic multilayer dielectric mirror. The critical coupling effect is robust, and the frequency where 100% absorption occurs can be easily tuned by adjusting either the slab thickness or the lattice period. Finally, a single structure can exhibit multiple resonances all satisfying the critical coupling condition, a capability that is potentially useful for multispectral photo-detection.

The paper is structured as follows. In the Theoretical Considerations section, we review the theory behind geometries for absorption enhancement in thin films and give a brief review of the concepts of guided resonance and critical coupling. In the Conditions To Achieve Critical Coupling section, we present an example of total absorption in graphene in the near-infrared and discuss the requirements to achieve this. In the Control of Critical Coupling section, we discuss the control of critical coupling in this structure and show several additional examples of total absorption. Finally, we give some details on methods in the Materials and Methods section.

THEORETICAL CONSIDERATIONS

One-Dimensional Geometries for Absorption Enhancement in a Thin Film. Before we discuss our results, we present an overview of some of the methods and considerations for enhancing absorption in a deep subwavelength layer. In particular, we begin by focusing on layered structures, where each layer is infinite in two dimensions, but has a finite thickness in the third (“transverse”) dimension. Such structures can be referred to as one-dimensional, since the translational symmetry is only broken along the transverse dimension. For simplicity, we consider a wave normally incident on the film, as shown in Figure 2.

It has long been known that the maximum single-pass absorption of a thin absorbing layer in air is 50%.^{26,27} The film in air is a two-port system. Light can be injected from either side of the structure; each side then constitutes a port. For a very thin film, one can understand the 50% absorption limit from a symmetry argument: a single wave incident from one side can be decomposed into a superposition between an even mode, where equal amplitude waves with the same phase illuminate the film from both sides, and an odd mode, where the two input waves are 180° out of phase. Only the even mode can contribute to the absorption: since the odd mode has vanishing fields at the thin film, it cannot contribute to the absorption. A wave incident from one side has equal power in the even and odd modes, and therefore the maximum absorption for single illumination cannot exceed 50%. The

absorption of monolayer graphene falls well below the theoretical limit in the visible and near-infrared, at around 2.3%.

More recently it was pointed out that a thin lossy slab illuminated from both sides can act as a coherent perfect absorber, absorbing all the incident light.²⁸ This is illustrated in Figure 2a. In this case, the condition for total absorption is that the determinant of S is zero, where S is the scattering matrix of the absorbing layer. This condition is equivalent to $|r| = |t|$. Considering that in the visible and near-infrared $|t|^2 \approx 0.97$ and $|r|^2 \approx 0$ for monolayer graphene in air, one cannot construct a coherent perfect absorber from monolayer graphene.

In order to overcome the 50% limit for a thin film illuminated by a single source, the simplest scheme is to add a mirror to the system. This changes the system from a two-port system to a one-port system, since the film can be accessed by the incident wave from only one side. In this case, the reflection off the front of the film can be canceled by the wave exiting the cavity made by the film and back mirror, as illustrated in Figure 2b.

Certain lossy films are amenable to this kind of critical coupling, where putting them on a dielectric spacer backed with a mirror is enough to achieve total absorption.²⁹ In fact, the condition for achieving complete absorption in the geometry of Figure 2b can be expressed in the simple form $|r| = |r^2 - t^2|$, where r and t are the Fresnel reflection and transmission coefficients of the thin film. (When including a spacer, with $n \neq 1$, the condition is modified to $|r_1| = |r_1 r_2 - t_1 t_2|$, where r_1 is the reflection coefficient from the front of the film–spacer pair and t_2 is the transmission from the spacer through the film.) For graphene in the visible and near-infrared, the condition for simple critical coupling cannot be satisfied. Therefore, one in fact cannot achieve total absorption in graphene in this way, as evidenced by a recent numerical study.³⁰

To achieve total absorption in graphene, the conceptually simplest method is to place the film inside an asymmetric Fabry–Perot cavity, with a perfect back mirror and a partially transmitting front mirror, as shown in Figure 2c. Total absorption occurs when the absorption rate in the film is equal to the rate at which energy enters the cavity, or (roughly speaking) $|t|^2 = A$, where t is the transmission of the front mirror in the absence of the cavity and A is the absorption of the film. The exact analytic condition for this case is complicated if expressed in terms of the indices and thicknesses of the layers since it is a five-layer problem. Also, the fabrication can be difficult, since it may involve growing a multilayer dielectric mirror on top of graphene.

Guided Resonance of Photonic Crystal Slabs. If one is willing to leave the relative simplicity of one-dimensional problems and their analytic descriptions, one can instead employ a photonic crystal slab as the resonator, in a one-port configuration with a mirror, as illustrated in Figure 1. In a

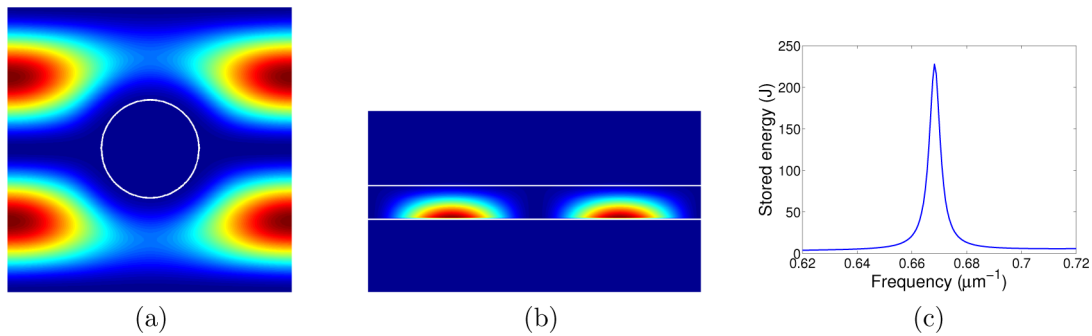


Figure 3. Distribution of $|E|^2$ and stored energy for a guided resonance at $1.5 \mu\text{m}$ in a photonic crystal slab on a lossless metallic mirror (structure of Figure 1a). The boundaries of the air hole and the slab are indicated in white. The silicon photonic crystal slab ($\epsilon = 12.1$) has lattice period $\Lambda = 900$ nm, thickness $d = 90$ nm, and hole radius $r = 0.17\Lambda = 153$ nm. Panel a shows $|E|^2$ at its maximum in the plane of the periodicity, while panel b shows a cross-section at the edge of the unit cell. The region below the slab is lossless metal. Panel c shows the stored energy in one unit cell of the slab (for an input power of 1 W per unit cell) as a function of frequency in the vicinity of the guided resonance. The resonance has a Q of 280.

photonic crystal slab, a correct choice of the in-plane periodicity enables phase-matched coupling between a guided mode and free-space radiation, creating a guided resonance.^{19–21} In the vicinity of the frequency of a guided resonance, the field inside the film can be significantly enhanced.

The field distribution for a guided resonance in the resonator given in Figure 1a, though without the graphene layer, is shown in Figure 3. The silicon photonic crystal slab ($\epsilon = 12.1$) has lattice period $\Lambda = 900$ nm, thickness $d = 90$ nm, and hole radius $r = 0.17\Lambda = 153$ nm, and the system is illuminated from above by a plane wave at $\lambda = 1.5 \mu\text{m}$. Figure 3a shows $|E|^2$ at its maximum in the plane of the photonic crystal (just above the mirror), and Figure 3b shows $|E|^2$ in cross-section at the edge of the unit cell. The air hole and the slab boundaries are indicated by the white lines. The peak field magnitude inside the slab is enhanced by a factor of 4.3×10^4 over the incident wave amplitude, while the peak field magnitude at the face of the slab is enhanced by 1.4×10^3 . The energy stored in one unit cell of the slab as a function of frequency is shown in Figure 3c. The normalized input power is 1 W per unit cell. This resonance has a Q of ~ 280 .

If a thin lossy film with $T \approx 1$ is placed on the photonic crystal slab, it has little impact on the light entering the slab or on the field distribution inside the slab. For example, if we include graphene in the system of Figure 1a, the pattern of the field distribution on resonance inside the photonic crystal slab is largely unchanged; however, the enhancement factors both inside the slab and at the slab surface (where the graphene layer sits) drop by a factor of 4 each, to 1.1×10^4 and 350, respectively. When the leakage rate of the guided resonance out of the slab is equal to the absorption rate in the film, we have critical coupling, and all incident power is absorbed. We emphasize that the phenomena of critical coupling is completely general and could be applied to any lossy atomically thin film, not just graphene.

As a side note, critical coupling to graphene can also be accomplished in a two-port system utilizing an all-pass photonic crystal filter,³¹ with additional structural complexity. In this paper we focus on the geometries of Figure 1.

Review of Coupled Mode Theory. In this paper we will account for the numerical simulations of the structures of Figure 1 using the coupled mode theory formalism. Coupled mode theory is used to describe the input–output properties of a resonator,³² where direct and indirect pathways interfere coherently. This formalism can account for both enhancement

and suppression of absorption, as well as the asymmetric Fano line shape.³³ We consider a resonator such as those shown in Figure 1 with stored energy $|a|^2$ in a single resonance at ω_0 , which interacts with input and output waves of amplitude u and y , respectively, with the power given by $|u|^2$ and $|y|^2$. The direct pathway corresponds to reflection from the structure without the excitation of the resonance, whereas the indirect pathway consists of resonant excitation.

For a lossless resonator, we are free to choose our reference plane so that the reflection coefficient from the direct pathway is -1 . If the time rate of amplitude change in the resonator with no input wave is given by the external leakage rate γ_e , then it can be shown by energy conservation and time reversibility arguments that the energy transfer rate between the incoming wave and the cavity and between the outgoing wave and the cavity are both proportional to $2\gamma_e$, with the phase fixed to be real by our choice of the background reflection coefficient. Then in the presence of material loss in the cavity as characterized by a small intrinsic loss rate δ , the system can be described by the equations

$$\dot{a} = (j\omega_0 - \gamma_e - \delta)a + \sqrt{2\gamma_e}u \quad (1)$$

$$y = \sqrt{2\gamma_e}a - u \quad (2)$$

This gives us the reflection coefficient

$$\Gamma \equiv \frac{y}{u} = \frac{j(\omega - \omega_0) + \delta - \gamma_e}{j(\omega - \omega_0) + \delta + \gamma_e} \quad (3)$$

and the absorption $A = 1 - |\Gamma|^2$:

$$A = \frac{4\delta\gamma_e}{(\omega - \omega_0)^2 + (\delta + \gamma_e)^2} \quad (4)$$

From eq 3, we see that when the system is driven on resonance ($\omega = \omega_0$), and the external leakage and intrinsic loss rates are the same ($\gamma_e = \delta$), then the reflection coefficient vanishes, and all incident power is absorbed.

In this paper we will use the guided resonance to achieve critical coupling to graphene. While critical coupling is not a new phenomena, photonic crystal guided resonances provide a particularly effective mechanism for critical coupling into graphene. The high transmittance and low single-pass absorption of graphene in this regime minimally perturb the behavior of the underlying resonator. Therefore, to design for critical coupling, one can focus attention on the design of the

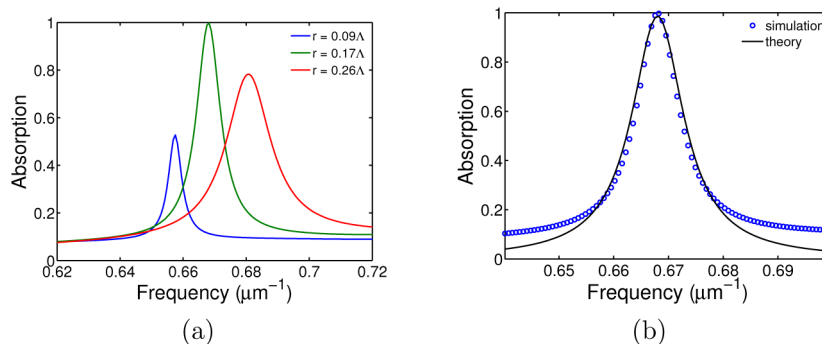


Figure 4. Demonstration and analysis of critical coupling. The simulated structure is shown in Figure 1a. The Si photonic crystal slab ($\epsilon = 12.1$) has lattice spacing $\Lambda = 900$ nm and thickness 90 nm and is backed by a lossless metallic mirror. Panel a shows the transition from undercoupling, through critical coupling, to overcoupling, by adjusting hole radius r . Total absorption occurs at $1.5 \mu\text{m}$, for $r = 0.17\Lambda = 153$ nm. The critically coupled resonance is analyzed using coupled mode theory in panel b. The excellent fit in the vicinity of the resonance validates the theory.

photonic crystal itself. Also, since graphene absorption in this regime is largely independent of frequency, the placement of the guided resonance frequency is not crucial; instead, controlling the external leakage rate is sufficient to achieve critical coupling. In the photonic crystal slab structure, the external leakage rate is controlled by the ratio of the hole radius to the periodicity r/Λ , and therefore simply tuning the radius itself is sufficient to achieve critical coupling, as we will demonstrate in the next section. Moreover, once r/Λ is chosen, the location of the total absorption can be adjusted over a wide range of frequencies by adjusting either the thickness d or the lattice period Λ , while leaving r/Λ fixed, as we demonstrate in the Control of Critical Coupling section.

■ CONDITIONS TO ACHIEVE CRITICAL COUPLING

Critical coupling is demonstrated in Figure 4a (green curve) for graphene on a photonic crystal slab backed by a lossless metallic mirror (the structure of Figure 1a). The slab is silicon ($\epsilon = 12.1$) with an array of air holes on a square lattice, with lattice constant $\Lambda = 900$ nm, thickness $d = 90$ nm, and hole radius $r = 0.17\Lambda = 153$ nm. In addition to being easy to fabricate, square lattice photonic crystals have the attractive property of being polarization-independent at normal incidence, due to their 90° rotational symmetry. The total absorption occurs at $0.667 \mu\text{m}^{-1}$, or $1.5 \mu\text{m}$, and the line width (full width at half-maximum) is $0.0064 \mu\text{m}^{-1}$, or 14 nm.

In order to achieve total absorption, several design principles were considered in the system design.

First, the backing mirror should be as close to perfect as possible, since any transmission through it represents energy leakage out of the system, and this energy therefore cannot be absorbed. For the result in Figure 4a, we used a lossless metal mirror. (We demonstrate critical coupling with a dielectric mirror in the Control of Critical Coupling) section.

Second, the lattice constant Λ , in addition to the requirement for enabling an incident wave to excite a guided resonance, must be smaller than the wavelength of interest. In our design, we chose $\Lambda = 900$ nm, to stay below the target wavelength of $1.5 \mu\text{m}$. The lattice of air holes acts as a 2-D grating. Any diffraction orders beyond 0 will scatter the incident light off normal and thus provide unrecoverable loss channels in a planar structure. In contrast, for our choice of a subwavelength grating, only the zero-order (forward) mode will propagate. All higher orders will be evanescent.

Finally, for ease of tuning, it is advantageous to keep the resonator modes to zero-order in the transverse (thickness)

direction. A lower-order guided resonance mode has a better overlap with the graphene layer compared with higher-order modes and hence a larger intrinsic loss rate δ . Consequently, using a lower-order guided resonance to achieve critical coupling requires a lower external quality factor, which increases the operating bandwidth and provides better tolerance to fabrication errors. Therefore, in our design we chose the slab to be 90 nm thick, a factor of 10 less than Λ , to ensure that higher-order transverse modes are cut off.

The critically coupled spectrum is compared to the results from coupled-mode theory in Figure 4b. We fit the spectrum of the total energy stored near a guided resonance as a Lorentzian function of frequency. For the slab without graphene, the center frequency of the Lorentzian gives the resonance frequency ω_0 , and the half-width at half-maximum gives the external leakage rate γ_e . When we repeat the calculation with graphene, the half-width at half-maximum gives us $\gamma_e + \delta$, and hence we obtain the intrinsic loss rate δ . Once the parameters are obtained, we verify them by calculating the system absorption using eq 4. In the vicinity of the resonance, coupled mode theory models the system very well, as shown in Figure 4b. The deviation between the theory and the simulation occurs only in the regions away from resonance, since the theory assumes a lossless direct (nonresonant) pathway and gives zero loss away from the resonance. Our results therefore indicate that coupled mode theory can provide an adequate description for the design of critical coupling in this system.

■ CONTROL OF CRITICAL COUPLING

In the photonic crystal guided resonance system, the external leakage rate γ_e is mostly controlled by the ratio r/Λ between the radius of the holes and the periodicity. Therefore, adjusting r/Λ enables us to tune through critical coupling, as shown in Figure 4a. For a fixed periodicity $\Lambda = 900$ nm, as r is increased from 81 nm to 234 nm, the external leakage rate γ_e increases. As a result, the total resonant line width $\gamma_e + \delta$ increases as seen in Figure 4a, since the intrinsic loss rate δ of the resonance is largely independent of the radius. In this range of radius, the system evolves from undercoupling, through critical coupling, to the overcoupling regime. Adjusting r also changes the resonant frequency of the system; increasing the hole radius pushes the resonance frequency higher.

Once we have achieved critical coupling by radius tuning, we can adjust the resonance frequency by changing the thickness d and/or the lattice period Λ , while maintaining the same r/Λ ratio. This is possible because the external leakage rate γ_e of the

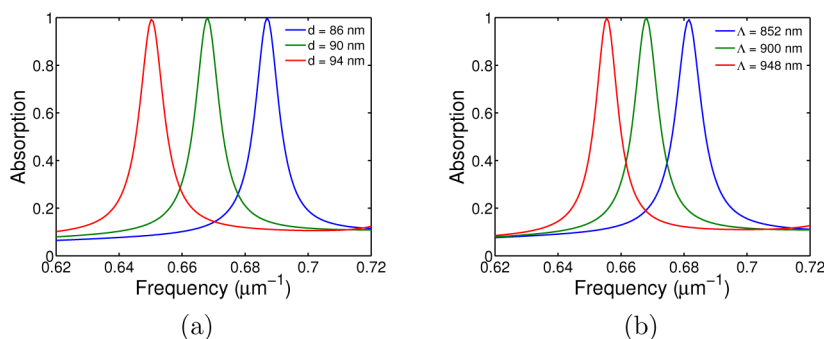


Figure 5. Adjusting the location of the guided resonance while maintaining critical coupling. (a) $\Lambda = 900$ nm and $r/\Lambda = 0.17$ while d is allowed to vary. (b) $d = 90$ nm and $r/\Lambda = 0.17$, while Λ is allowed to vary. Due to the relatively stable resonance Q and graphene's constant absorption, the normalized hole radius does not need to be retuned in order to maintain critical coupling.

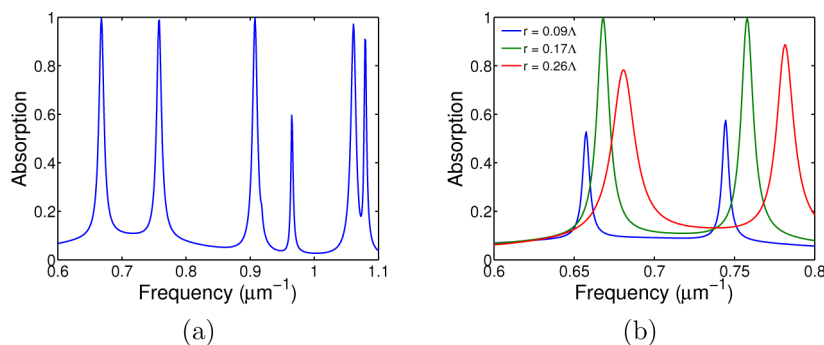


Figure 6. Multiple resonances can be simultaneously tuned through critical coupling. The silicon slab has $\Lambda = 900$ nm, thickness $d = 90$ nm, and hole radius $r = 0.17\Lambda = 153$ nm. The spectrum is shown in panel a, with several critically coupled peaks visible. Simultaneous tuning of two adjacent resonances through critical coupling by adjusting the hole radius is shown in panel b.

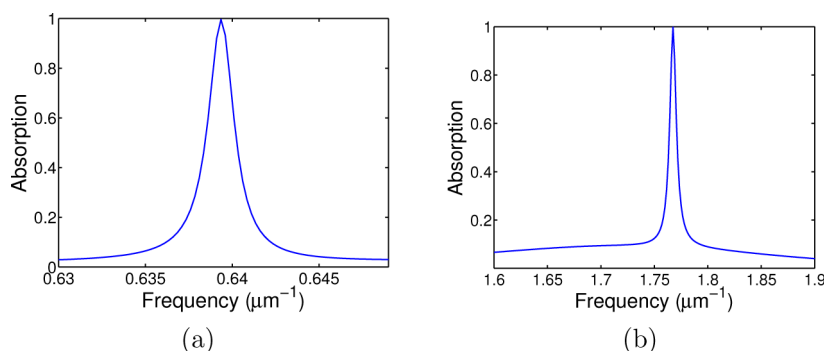


Figure 7. (a) Total absorption for a silicon photonic crystal with 5.5-pair dielectric Bragg mirror, as illustrated in Figure 1b. The photonic crystal has $d = 90$ nm, $\Lambda = 900$ nm, and $r = 0.21\Lambda = 189$ nm. (b) Critical coupling in the visible ($\lambda = 566$ nm), using Ta_2O_5 photonic crystal ($\epsilon = 4.4$) and lossless metallic mirror. This system has $d = 220$ nm, $\Lambda = 390$ nm, and $r = 0.317\Lambda = 123$ nm.

zero-order resonances is relatively stable with respect to either d or Λ , and the absorption of graphene is essentially independent of frequency in this regime. These factors combine to provide a nearly ideal example of critical coupling.

As thickness is increased, the resonance frequency is pushed down, as shown in Figure 5a. Similarly, increasing Λ pushes the resonance to longer wavelength (lower frequency), as shown in Figure 5b. In both cases, critical coupling is maintained in spite of significant change of the resonant frequencies. In Figure 5, the frequency of total absorption is shifted by the same amount as in Figure 4a, by changing the thickness by $\pm 4\%$ (Figure 5a) or the lattice spacing by $\pm 6\%$ (Figure 5b) while maintaining critical coupling. In Figure 5a, the frequency of total absorption is tuned over a range of $4\gamma_c$, which shows that the critical coupling is a fairly robust effect for such a resonant system.

Figure 6a shows the spectrum for the same system as in Figure 4b, with $\Lambda = 900$ nm, $r/\Lambda = 0.17$, and $d = 90$ nm, but over a broader frequency range. As can be seen, there are two resonances that are critically coupled and several others that are close. Due to the frequency-independent absorption of graphene and the stable Q of these resonances, one can simultaneously tune the leftmost two resonances through critical coupling, as shown in Figure 6b. Therefore, we have shown that a single structure can simultaneously achieve critical coupling at multiple resonances, which is an important consideration for multispectral light detection.

In this paper up to now, we have chosen a lossless metallic mirror for simplicity. Here we show that the same critical coupling effect can be achieved with a more realistic dielectric Bragg mirror as well. Figure 7a shows critical coupling for the

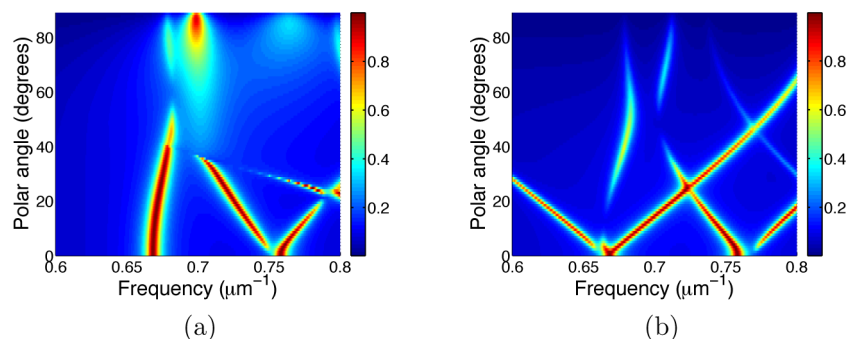


Figure 8. Absorption spectra as a function of frequency and angle of incidence, for the critically coupled structure of Figure 4. (a) Spectrum for s-polarization, where the electric field is perpendicular to the plane of incidence, and (b) spectrum for p-polarization, where the electric field is parallel to the plane of incidence. In both cases, the tangential wave vector of the incident plane wave is oriented along the [10] direction. For s-polarization, the mode at $0.667 \mu\text{m}^{-1}$ is fairly robust and exhibits minimal frequency shift as the angle of incidence is increased, until it is cut off around 40° .

structure illustrated in Figure 1b. Using $d = 90 \text{ nm}$, $\Lambda = 900 \text{ nm}$, and $r = 0.21\Lambda = 189 \text{ nm}$, we can achieve $A = 0.996$ by using a Bragg mirror with only 5.5 pairs, composed of alternate layers of Si ($\epsilon = 12.1$) and SiO_2 ($\epsilon = 2.1$). The mirror is centered at $\lambda_0 = 1.5 \mu\text{m}$, and the layer thicknesses were chosen as $\lambda_0/4n$, where n is the refractive index of the layer in question. Using this Bragg mirror, the total system is under $2 \mu\text{m}$ thick, or just over $4/3$ free-space wavelength. In practice, the use of a dielectric Bragg mirror is likely preferable to the use of a real metal mirror (for example a few hundred nanometers of Au), because the proximity of the metal to the photonic crystal can easily lead to parasitic absorption in the metal exceeding the absorption in the graphene.

For illustration purposes we have focused on the near-infrared wavelength range near $1.5 \mu\text{m}$. The same critical coupling concept applies equally to the visible wavelength range, in spite of the fact that the available range of index contrast for lossless dielectrics is much larger in the near-infrared. In Figure 7b, we give an example of total absorption at $1.767 \mu\text{m}^{-1}$, or 566 nm . The losses in silicon become appreciable for wavelengths shorter than about $1 \mu\text{m}$, and silicon becomes opaque in the visible. Therefore, we used tantalum pentoxide (Ta_2O_5) for the photonic crystal, which is lossless in this regime, but has a relatively high dielectric constant ($\epsilon = 4.5$). The structure in Figure 7b has $d = 220 \text{ nm}$, $\Lambda = 390 \text{ nm}$, and $r = 0.317\Lambda = 123 \text{ nm}$, backed by a lossless metallic mirror.

Finally, in Figure 8 we show the angular dependence of the critically coupled structure from Figure 4a. We fix the parallel component of the wave vector of the incident plane wave to be along the [10] direction, but vary the angle of incidence for the input beam, for both s-polarization (electric field perpendicular to the plane of incidence; Figure 8a) and p-polarization (electric field parallel to the plane of incidence; Figure 8b). For both polarizations, there are broad angular ranges where strong absorption occurs. For the s-polarized case, the lowest-order resonance near $0.667 \mu\text{m}^{-1}$ ($1.5 \mu\text{m}$) exhibits minimal frequency shift as a function of angle, until around 40° , while the higher-order resonance near $0.75 \mu\text{m}^{-1}$ exhibits frequency splitting. In contrast, for p-polarization (Figure 8b), both resonances exhibit frequency splitting and a substantial shift of resonance as a function of angle.

In conclusion, we have shown that through the use of a photonic crystal resonator, the absorption of monolayer graphene can reach 100% in the near-infrared and visible, through the mechanism of critical coupling. The system under

study has robust performance, is simple to fabricate, and can be made in an all-dielectric (lossless) form. The present work could be directly applied in the design of advanced photo-detectors and modulators with tiny dimensions. In addition, the concept could be extended to other two-dimensional materials, such as graphene (in which an H atom is chemically bonded to each C atom) or MoS_2 .

MATERIALS AND METHODS

Graphene can be modeled either as a conductive film with complex conductivity and vanishing thickness or as a thin anisotropic layer with complex refractive index in-plane, and $n = 1$ in the transverse direction. (In practice, the thickness is so small that the anisotropy can in general be ignored.) In our calculations we used the latter approach, with $n = 3 + j5.446\lambda/3 \mu\text{m}^{-1}$ for the refractive index of graphene.³⁴ The graphene thickness is taken as 0.34 nm . All simulations in this work were performed using the S^4 implementation³⁵ of the rigorous coupled wave analysis (RCWA) method.³⁶ We used $\epsilon = 12.1$ for silicon, $\epsilon = 2.1$ for SiO_2 , and $\epsilon = 4.5$ for Ta_2O_5 .

Here we assumed that there is no Pauli state-blocking effect near the wavelength of $1.5 \mu\text{m}$. Xia¹³ has noted that with a chemical potential of -350 meV , as appropriate for an as-prepared graphene sample grown by chemical vapor deposition, the Pauli state-blocking effect becomes significant for wavelengths longer than $1.43 \mu\text{m}$, slightly reducing graphene's single-pass absorption. We expect that such Pauli state-blocking effects can be suppressed at $1.5 \mu\text{m}$ through a different choice of chemical potential. Furthermore, by dynamically adjusting the chemical potential via electrostatic gating, the total absorption in the critically coupled resonator could be modulated, since adjusting the lossy layer's optical properties can move the system either toward or away from the critical coupling condition, thereby providing strong modulation of the absorption.

AUTHOR INFORMATION

Corresponding Authors

*E-mail: jrylan@stanford.edu.

*E-mail: shanhui@stanford.edu.

Notes

The authors declare no competing financial interest.

ACKNOWLEDGMENTS

This work is supported in part by an AFOSR MURI program Grant No. FA9550-12-0024. J.R.P. is additionally supported by the Robert and Ruth Halperin Stanford Graduate Fellowship.

REFERENCES

- (1) Bonaccorso, F.; Sun, Z.; Hasan, T.; Ferrari, A. C. Graphene photonics and optoelectronics. *Nat. Photonics* **2010**, *4*, 611–622.
- (2) Grigorenko, A. N.; Polini, M.; Novoselov, K. S. Graphene plasmonics. *Nat. Photonics* **2012**, *6*, 749–758.
- (3) Bao, Q.; Loh, K. P. Graphene photonics, plasmonics, and broadband optoelectronic devices. *ACS Nano* **2012**, *6*, 3677–3694.
- (4) Liu, M.; Yin, X.; Ulin-Avila, E.; Geng, B.; Zentgraf, T.; Ju, L.; Wang, F.; Zhang, X. A graphene-based broadband optical modulator. *Nature* **2011**, *474*, 64–67.
- (5) Xia, F.; Mueller, T.; Lin, Y.-M.; Valdes-Garcia, A.; Avouris, P. Ultrafast graphene photodetector. *Nat. Nanotechnol.* **2009**, *4*, 839–843.
- (6) Gan, X.; Shiue, R.-j.; Gao, Y.; Meric, I.; Heinz, T. F.; Shepard, K.; Hone, J.; Assefa, S.; Englund, D. Chip-integrated ultrafast graphene photodetector with high responsivity. *Nat. Photonics* **2013**, *7*, 883–887.
- (7) Gao, W.; Shu, J.; Qiu, C.; Xu, Q. Excitation of plasmonic waves in graphene by guided-mode resonances. *ACS Nano* **2012**, *6*, 7806–7813.
- (8) Zhan, T. R.; Zhao, F. Y.; Hu, X. H.; Liu, X. H.; Zi, J. Band structure of plasmons and optical absorption enhancement in graphene on subwavelength dielectric gratings at infrared frequencies. *Phys. Rev. B* **2012**, *86*, 165416.
- (9) Zhu, X.; Yan, W.; Uhd Jepsen, P.; Hansen, O.; Asger Mortensen, N.; Xiao, S. Experimental observation of plasmons in a graphene monolayer resting on a two-dimensional subwavelength silicon grating. *Appl. Phys. Lett.* **2013**, *102*, 131101.
- (10) Christensen, J.; Manjavacas, A.; Thongrattanasiri, S.; Koppens, F. H. L.; de Abajo, F. J. G. Graphene plasmon waveguiding and hybridization in individual and paired nanoribbons. *ACS Nano* **2012**, *6*, 431–440.
- (11) Thongrattanasiri, S.; Koppens, F. H. L.; García de Abajo, F. J. Complete Optical Absorption in Periodically Patterned Graphene. *Phys. Rev. Lett.* **2012**, *108*, 047401.
- (12) Fang, Z.; Thongrattanasiri, S.; Schlather, A.; Liu, Z.; Ma, L.; Wang, Y.; Ajayan, P. M.; Nordlander, P.; Halas, N. J.; García de Abajo, F. J. Gated tunability and hybridization of localized plasmons in nanostructured graphene. *ACS Nano* **2013**, *7*, 2388–2395.
- (13) Xia, F.; Yan, H.; Avouris, P. The Interaction of Light and Graphene: Basics, Devices, and Applications. *Proc. IEEE* **2013**, *101*, 1717–1731.
- (14) Nair, R. R.; Blake, P.; Grigorenko, A. N.; Novoselov, K. S.; Booth, T. J.; Stauber, T.; Peres, N. M. R.; Geim, A. K. Fine structure constant defines visual transparency of graphene. *Science* **2008**, *320*, 1308.
- (15) Fang, Z.; Liu, Z.; Wang, Y.; Ajayan, P. M.; Nordlander, P.; Halas, N. J. Graphene-antenna sandwich photodetector. *Nano Lett.* **2012**, *12*, 3808–3813.
- (16) Furchi, M.; Urich, A.; Pospischil, A.; Lilley, G.; Unterrainer, K.; Detz, H.; Klang, P.; Andrews, A. M.; Schrenk, W.; Strasser, G.; Mueller, T. Microcavity-integrated graphene photodetector. *Nano Lett.* **2012**, *12*, 2773–2777.
- (17) Ferreira, A.; Peres, N. M. R.; Ribeiro, R. M.; Stauber, T. Graphene-based photodetector with two cavities. *Phys. Rev. B* **2012**, *85*, 115438.
- (18) Yariv, A. Critical coupling and its control in optical waveguide-resonator systems. *IEEE Photonic Technol. Lett.* **2002**, *14*, 483–485.
- (19) Fan, S.; Joannopoulos, J. Analysis of guided resonances in photonic crystal slabs. *Phys. Rev. B* **2002**, *65*, 235112.
- (20) Astratov, V.; Culshaw, I. Resonant coupling of near-infrared radiation to photonic band structure waveguides. *J. Lightwave Technol.* **1999**, *17*, 2050–2057.
- (21) Wang, S. S.; Magnusson, R.; Bagby, J. S.; Moharam, M. G. Guided-mode resonances in planar dielectric-layer diffraction gratings. *J. Opt. Soc. Am. A* **1990**, *7*, 1470–1474.
- (22) Hsu, C. W.; Zhen, B.; Lee, J.; Chua, S.-L.; Johnson, S. G.; Joannopoulos, J. D.; Soljačić, M. Observation of trapped light within the radiation continuum. *Nature* **2013**, *499*, 188–191.
- (23) Yang, H.; Zhao, D.; Chuwongin, S.; Seo, J.-h.; Yang, W.; Shuai, Y.; Berggren, J.; Hammar, M.; Ma, Z.; Zhou, W. Transfer-printed stacked nanomembrane lasers on silicon. *Nat. Photonics* **2012**, *6*, 617–622.
- (24) Norton, S. M.; Erdogan, T.; Morris, G. M. Coupled-mode theory of resonant-grating filters. *J. Opt. Soc. Am. A* **1997**, *14*, 629–639.
- (25) Tamir, T.; Zhang, S. Resonant scattering by multilayered dielectric gratings. *J. Opt. Soc. Am. A* **1997**, *14*, 1607–1616.
- (26) Hadley, L. N.; Dennison, D. M. Reflection and transmission interference filters. *J. Opt. Soc. Am.* **1947**, *37*, 451–465.
- (27) Botten, L. C.; McPhedran, R. C.; Nicorovici, N. A.; Derrick, G. H. Periodic models for thin optimal absorbers of electromagnetic radiation. *Phys. Rev. B* **1997**, *55*, R16072–R16082.
- (28) Chong, Y.; Ge, L.; Cao, H.; Stone, A. Coherent perfect absorbers: time-reversed lasers. *Phys. Rev. Lett.* **2010**, *105*, 053901.
- (29) Tischler, J. R.; Bradley, M. S.; Bulović, V. Critically coupled resonators in vertical geometry using a planar mirror and a 5 nm thick absorbing film. *Opt. Lett.* **2006**, *31*, 2045–2047.
- (30) Liu, J.-T.; Liu, N.-H.; Li, J.; Jing Li, X.; Huang, J.-H. Enhanced absorption of graphene with one-dimensional photonic crystal. *Appl. Phys. Lett.* **2012**, *101*, 052104.
- (31) Suh, W.; Fan, S. All-pass transmission or flat-top reflection filters using a single photonic crystal slab. *Appl. Phys. Lett.* **2004**, *84*, 4905–4907.
- (32) Haus, H. A. *Waves and Fields in Optoelectronics*; Prentice Hall: Englewood Cliffs, NJ, 1984.
- (33) Fan, S.; Suh, W.; Joannopoulos, J. Temporal coupled-mode theory for the Fano resonance in optical resonators. *J. Opt. Soc. Am. A* **2003**, *20*, 569–572.
- (34) Bruna, M.; Borini, S. Optical constants of graphene layers in the visible range. *Appl. Phys. Lett.* **2009**, *94*, 031901.
- (35) Liu, V.; Fan, S. S4: A free electromagnetic solver for layered periodic structures. *Comput. Phys. Commun.* **2012**, *183*, 2233–2244.
- (36) Moharam, M. G.; Gaylord, T. K. Rigorous coupled-wave analysis of planar-grating diffraction. *J. Opt. Soc. Am.* **1981**, *71*, 811–818.